IEEE Photonics Journal
An IEEE Photonics Society Publication

Open Access

Polarization-Maintaining Single-Frequency Fiber Laser With Quadruple Wavelengths at the C-Band

Volume 10, Number 5, September 2018

Kunyi Li
Huaqiu Deng
Pengfei Ma
Wei Lin
Huihui Cheng
Xianchao Guan
Changsheng Yang
Qilai Zhao
Yuning Zhang
Zhongmin Yang
Shanhui Xu

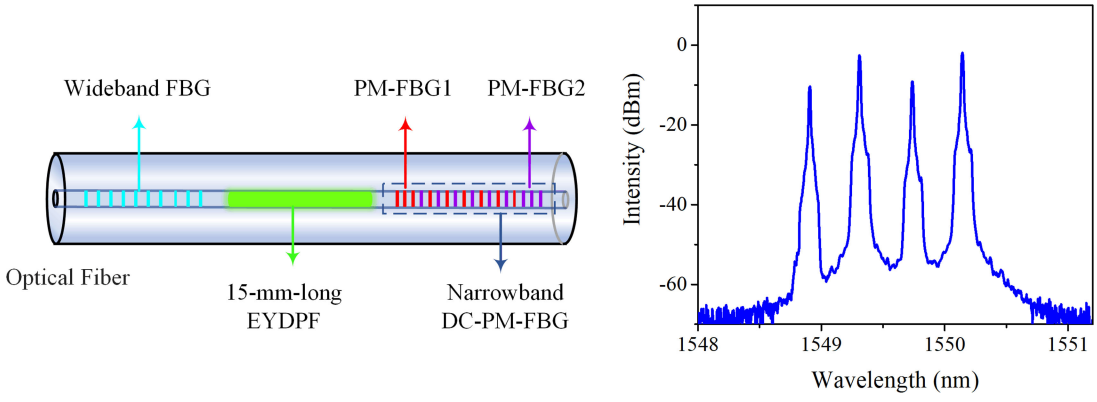

DOI: 10.1109/JPHOT.2018.2871076
1943-0655

Polarization-Maintaining Single-Frequency Fiber Laser With Quadruple Wavelengths at the C-Band

Kunyi Li,[1,2,3] Huaqiu Deng,[1,2,3] Pengfei Ma,[1] Wei Lin,[1] Huihui Cheng,[1] Xianchao Guan,[1] Changsheng Yang,[1,3,4,5] Qilai Zhao,[1] Yuning Zhang,[1] Zhongmin Yang,[1,2,3,4,5] and Shanhui Xu [1,3,4,5]

[1]State Key Laboratory of Luminescent Materials and Devices and Institute of Optical Communication Materials, South China University of Technology, Guangzhou 510640, China
[2]School of Physics and Optoelectronics, South China University of Technology, Guangzhou 510640, China
[3]Guangdong Engineering Technology Research and Development Center of Special Optical Fiber Materials and Devices, Guangzhou 510640, China
[4]Guangdong Engineering Technology Research and Development Center of High-Performance Fiber Laser Techniques and Equipments, Zhuhai 519031, China
[5]Guangdong Provincial Key Laboratory of Fiber Laser Materials and Applied Techniques, South China University of Technology, Guangzhou 510640, China

DOI:10.1109/JPHOT.2018.2871076

Manuscript received June 13, 2018; revised July 28, 2018; accepted September 14, 2018. Date of publication September 19, 2018; date of current version October 8, 2018. This work was supported in part by the National Natural Science Foundation of China under Grants 61635004, 61535014, and 11674103, in part by the Major Program of the National Natural Science Foundation of China under Grant 61790582, in part by the Guangdong Natural Science Foundation under Grants 2016A030310410 and 2017A030310007, in part by the Science and Technology Project of Guangdong under Grants 2016B090925004, 2015B090926010, 2014B050505007, and 2017B090911005, and in part by the Science and Technology Program of Guangzhou under Grant 201804020028. *(Kunyi Li and Huaqiu Deng contributed equally to this work.)* Corresponding author: Shanhui Xu (e-mail: flxshy@scut.edu.cn).

Abstract: In this paper, a polarization-maintaining quad-wavelength (QW) single-frequency fiber laser (SFFL) at the C-band with the novel and compact structure is demonstrated. Applying the rate equations and multiple coupled nonlinear Schrödinger equations, the theoretical model of QW fiber lasers is established, and then the optical spectra, temporal evolution, and stability of the QW fiber laser are analyzed numerically. Based on the theoretical analysis, a QW-SFFL having an ultrashort linear distributed Bragg reflector cavity is proposed. Utilizing a wideband fiber Bragg grating coupled with a dual-channel polarization maintaining fiber Bragg grating as the wavelength selection and a 15-mm-long Er^{3+}/Yb^{3+} co-doped phosphate fiber as the gain medium has realized a robust QW laser with the wavelength spacing of 0.4 nm. All the wavelengths maintain the single-frequency operation independently with the linewidths of 20 kHz. This type of compact SFFLs with quadruple wavelengths is widely adapted to lidar systems and fiber sensing.

Index Terms: Optical fiber lasers, quadruple wavelengths, single-frequency.

1. Introduction

Multi-wavelength single-frequency fiber lasers (SFFLs) at the C-band have attracted great interest because of their extensive applications in, for example, lidar systems and fiber sensing [1]–[3]. In recent years, the implementation of multi-wavelength fiber laser scanners identification and discrimination for complex materials has become prevalent. The multi-wavelength laser scanning can be used to identify the features and materials of objects by measuring their reflectance characteristics at specific wavelengths and matching them with their spectral reflectance curves [4]. Moreover, differential absorption lidars, which are used to monitor trace gases, require two narrow-linewidth laser sources of nearly the same wavelength. The differential absorption at the two wavelengths results in different backscattered spectra and can be used to calculate the concentration of the gas [5]. Especially, based on the multi-wavelength lidars at 1.5 μm, numerous gases, such as acetylene and NH_3 can be measured [6], [7]. Using more than two wavelengths is an obvious extension of the lidar systems. In addition to measuring more than one gases simultaneously, multiple wavelengths may also provide better knowledge of aerosol optical properties, which will improve measurement accuracy [1]. Single-longitudinal-mode (SLM) operation is an ideal property for lidar sources as it ensures narrow linewidth [8]. Thus, lasers combining single-frequency with multi-wavelength are highly desirable in lidar systems and fiber sensing.

Wavelength selections in multi-wavelength lasers have been achieved by using fiber Sagnac loop, photonics crystal fiber, and fiber Bragg gratings (FBGs) in the resonant cavity [9], [10]. Coupling of the fiber loop and laser cavities impedes the SLM operation due to its long-cavity [11], in contrast, the FBG with compact structure and narrow bandwidth can be incorporated into a short cavity of the laser, which provides a wide space of longitude mode to ensure SLM operation [12], [13]. Specifically, the FBGs with different reflection wavelengths best to be engraved at the adjacent location on the fiber for the purpose of minimizing the cavity-length. However, a stable multi-wavelength lasing is hardly realized due to the strong mode competition and mode hopping caused by the homogeneous gain broadening of Er^{3+} [14]. To overcome this difficulty, polarization hole burning effect should be induced by using polarization maintaining (PM) components [15], [16], and nonlinear optical effects can be applied to regulate the wavelength-dependent gain of the resonant cavity, which is conducive to multiple-wavelength lasing [17], [18]. Currently, studies of SFFLs mainly focus on the single-wavelength operation [19], whereas the output performance with multiple wavelengths is rarely reported.

This paper presents a compact PM-SFFL with quadruple wavelengths based on a short linear resonant cavity. A reliable quad-wavelength (QW) SFFL with the wavelength spacing of 0.4 nm was obtained, and the linewidth of individual lasing wavelength was about 20 kHz.

2. Theoretical Analyses

2.1 Theory for Numerical Modeling

To obtain a stable multi-wavelength fiber laser, physical formation and interaction mechanisms of multi-wavelength laser in the resonant cavity are significant to be investigated. The evolution of optical fields in a multi-wavelength fiber laser comprises the power amplification and nonlinear propagation processes.

The process of power amplification in the active fiber is determined by the wavelength-dependent gain which is calculated by the steady-state rate equations. The laser action in Er^{3+}/Yb^{3+} co-doped phosphate fiber (EYDPF) can be described by a four-level system of Er^{3+} along with a two-level system of Yb^{3+} [20], [21]. On the basis of the energy level of Er^{3+}/Yb^{3+} co-doped system, the rate equations for Er^{3+} and Yb^{3+} population densities can be written as:

$$\frac{\partial N_2}{\partial t} = W_{12}N_1 + A_{32}N_3 - W_{21}N_2 - C_{tr}N_2N_6 - \frac{N_2}{\tau_{Er}} - 2C_{up}N_2^2 \quad (1)$$

$$\frac{\partial N_3}{\partial t} = C_{cr}N_1N_6 + A_{43}N_4 - A_{32}N_3 \quad (2)$$

$$\frac{\partial N_4}{\partial t} = C_{up} N_2^2 - A_{43} N_4 \tag{3}$$

$$\frac{\partial N_6}{\partial t} = W_{56} N_5 - \frac{N_6}{\tau_{Yb}} - W_{65} N_6 - C_{cr} N_1 N_6 - C_{tr} N_2 N_6 \tag{4}$$

$$N_{Er} = N_1 + N_2 + N_3 + N_4 \tag{5}$$

$$N_{Yb} = N_5 + N_6 \tag{6}$$

$$\frac{dp_p(z, \lambda_p)}{dz} = -\Gamma_p(\lambda_p)[\sigma_{56} N_5(z) - \sigma_{65} N_6(z)] p_p(z) - \alpha(\lambda_p) p_p(z, \lambda_p) \tag{7}$$

$$\frac{dp_s(z, \lambda_s)}{dz} = \Gamma_s(\lambda_s)[\sigma_{21} N_2(z) - \sigma_{12} N_1(z)] p_s(z, \lambda_s) - \alpha(\lambda_s) p_s(z, \lambda_s) \tag{8}$$

where N_1, N_2, N_3, and N_4 are the population density of Er^{3+} at ground state, metastable state, excited state, and upper state, respectively; N_5 and N_6 are the population density of Yb^{3+} at ground state and excited state; N_{Er} and N_{Yb} are the concentrations of Er^{3+} and Yb^{3+}; τ_{Er} and τ_{Yb} are the fluorescence lifetime of Er^{3+} and Yb^{3+}; W_{12} and W_{21} are the stimulated absorption rates and stimulated emission rates of Er^{3+}; W_{56} and W_{65} are the stimulated absorption rates and stimulated emission rates of Yb^{3+}, respectively; C_{up} is up-conversion coefficient from metastable state to excited state of Er^{3+}; C_{cr} is energy transfer coefficient; C_{tr} is cumulative up-conversion energy transfer coefficient; A_{43} and A_{32} are the Er^{3+} de-excitation rate from upper state to excited state and from excited state to metastable state, respectively; Γ_p and Γ_s are the power filling factor of the pump power and signal power; σ_{56} and σ_{65} are the absorption and emission cross section of Yb^{3+} at the pump wavelength; σ_{12} and σ_{21} are the absorption and emission cross section of Er^{3+} at signal wavelength.

By solving the rate equations of Er^{3+}/Yb^{3+} co-doped system, the gain coefficient of signal light can be derived and expressed as:

$$g_s = \Gamma_s(\omega_s)[\sigma_{21} N_2(z) - \sigma_{12} N_1(z)] \tag{9}$$

Subsequently, the process of the optical fields propagation in the fiber can be accurately simulated by nonlinear Schrödinger equations (NLSEs) [22]–[25], which takes into account the active gain, dispersion, and other nonlinear effects. Considering the multiple optical fields with different wavelengths in different polarization states will cause self-phase modulation and cross-phase modulation, the optical fields evolution inside active fiber is described by a set of multiple coupled NLSEs of the form:

$$\frac{\partial A_{jx}}{\partial z} + \beta_1 \frac{\partial A_{jx}}{\partial t} + \frac{i\beta_2}{2} \frac{\partial^2 A_{jx}}{\partial t^2} - i\gamma \left(|A_{jx}|^2 + 2 \sum_{k \neq j} |A_{kx}|^2 + \frac{2}{3} \sum |A_{ky}|^2 \right) A_{jx} = \frac{g_s}{2} A_{jx} \tag{10}$$

$$\frac{\partial A_{jy}}{\partial z} + \beta_1 \frac{\partial A_{jy}}{\partial t} + \frac{i\beta_2}{2} \frac{\partial^2 A_{jy}}{\partial t^2} - i\gamma \left(|A_{jy}|^2 + 2 \sum_{k \neq j} |A_{ky}|^2 + \frac{2}{3} \sum |A_{kx}|^2 \right) A_{jy} = \frac{g_s}{2} A_{jy} \tag{11}$$

where A_j is one propagating optical field, x and y correspond to two polarization states, z is the spatial coordinate along the fiber, t is retarded time, β_1 is the first-order dispersion coefficient, β_2 is the second-order dispersion coefficient, γ is the nonlinear parameter, and g_s is the gain coefficient.

Wavelength selections in fiber laser is mainly produced by the FBGs which are placed on both sides of the cavity, and the optical fields after reflection can be represented as:

$$A_{j,n}(0, \omega) = R_W(\omega) A_{j,n-1}(L, \omega) \tag{12}$$

$$A_{j,n+1}(0, \omega) = R_N(\omega) A_{j,n}(L, \omega) \tag{13}$$

where $R_W(\omega)$ is the reflectivity of wideband FBG, $R_N(\omega)$ is reflectivity of narrowband FBG, n is the single-pass number, L is the cavity length.

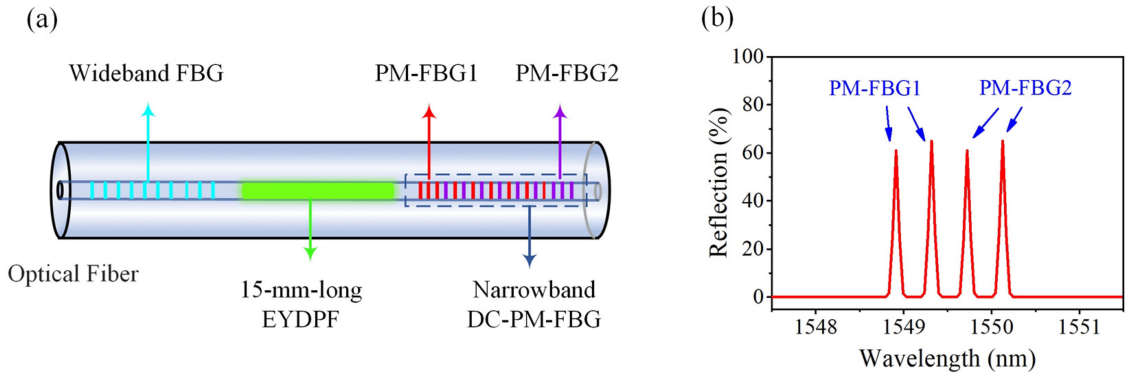

Fig. 1. (a) Schematic of simulated short-linear-cavity for QW-SFFL. (b) Representative simulated reflectivity of narrowband DC-PM-FBG. EYDPF, Er^{3+}/Yb^{3+} co-doped phosphate fiber; DC-PM-FBG, dual-channel polarization maintaining fiber Bragg grating.

The optical fields transmission model above is capable of describing the evolution of multi-wavelength laser in the resonant cavity. The laser generally starts with a slight disturbance of the spontaneous emission of active fiber, so that the initial signal in the cavity is supposed as Gaussian white noise signal in the frequency domain [24], and it can be transformed into the time domain conveniently during solving NLSEs. The multiple coupled NLSEs are solved with the split-step Fourier algorithm which discretizes the frequency domain by $\Delta f = 1/T$, where T is the width of the temporal window in the calculations. Such a frequency separation of the split-step Fourier method closely resembles the introduction of longitudinal modes in simulations. For the accurate simulation, therefore, Δf is designed to be in accord with the actual intervals of longitudinal modes. Besides, during the transmitting in the resonant cavity, each optical field of the single wavelength is regarded as the result from two independent amplification and propagation in opposite directions. Since the wavelengths of the individual beams are similar, the neglect of the group-velocity mismatch is allowed in this simulation.

Summarily, the numerical simulations were performed by first introducing Gaussian white noise into the laser cavity. The wavelength-dependent gain was accurately calculated from the steady-state rate equations, and the evolution of the optical fields along the fiber was obtained by solving the multiple coupled NLSEs with the split-step Fourier method [24]. The FBGs at both ends of active fiber would change the direction of transmission and select oscillating wavelengths. When the previous simulated optical fields were received, the results were used as the input for the next round transmission. After multiple round trips in the cavity, the main characteristics of optical fields including energy and spectrum would approach a stable value, and that was the last output required.

2.2 Simulation Results

The spectral and temporal properties of the QW fiber laser were simulated based on the theoretical model presented above. The resonant cavity adopted in the simulation, as described in Fig. 1(a), is constructed by installing a wideband FBG with the reflectivity of 99.5% and a narrowband dual-channel polarization maintaining FBG (DC-PM-FBG) on both ends of a 15-mm-long high gain EYDPF. One of a representative simulated reflectivity of DC-PM-FBG is shown in Fig. 1(b), where the reflection bandwidth is alterable in the simulation. There are four reflection bands in the DC-PM-FBG and the separation of reflection peaks is 0.4 nm. Table 1 shows the values of the major parameters used in the simulation.

To explore the impact of SLM operation on stability, we simulated the QW fiber laser operated in SLM and multiple-longitudinal-mode (MLM) by adjusting the bandwidth of narrowband FBG. The effective length of the resonant cavity is about 30 mm having the longitudinal mode spacing of

TABLE 1
The Related Parameters Used in the Simulations

Symbol	Value and units	Symbol	Value and units
C_{cr}	2.1×10^{-22} $m^3\cdot s^{-1}$	σ_{56}	1.01×10^{-24} m^2
C_{up}	2×10^{-24} $m^3\cdot s^{-1}$	σ_{65}	1.27×10^{-24} m^2
C_{tr}	0.85×10^{-22} $m^3\cdot s^{-1}$	σ_{12}	4.99×10^{-25} m^2
N_{Er}	8.74×10^{25} m^{-3}	σ_{21}	6.02×10^{-25} m^2
N_{Yb}	8.74×10^{25} m^{-3}	Γ_s	0.9
τ_{Er}	8.4×10^{-3} s	Γ_p	0.9
τ_{Yb}	2×10^{-3} s	P_p	200 mW
A_{43}	7×10^{9} s^{-1}	β_1	4.8×10^{-9} $s\cdot m^{-1}$
A_{32}	2.8×10^{6} s^{-1}	β_2	-20×10^{-27} $s^2\cdot m^{-1}$
λ_p	976 nm	γ	2.8 W^{-1} km^{-1}

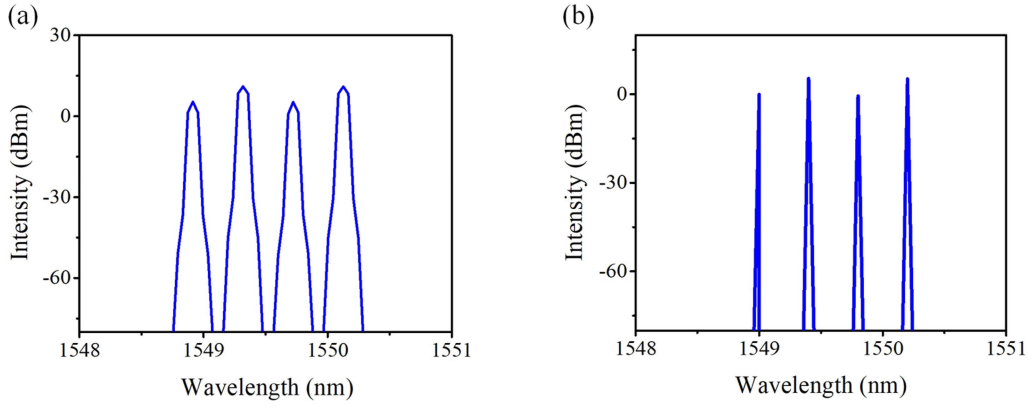

Fig. 2. Simulated spectrum of output laser in (a) MLM and (b) SLM operation.

3.4 GHz, accordingly, only one longitudinal mode is supported within each reflection peak when each reflection bandwidth of narrowband FBG is less than 6.8 GHz.

The initial width of individual wavelength in the simulation was assumed to be 0.5 nm, then the optical fields went through the iterations of rate equations and multiple coupled NLSEs. Eventually, the power of each spectral channel with respect to the QW lasing evolved into a duplicated quasi-periodic pattern after 80 round trips evolutions and the simulated spectra results are shown in Fig. 2. When the reflection bandwidth of narrowband FBG was assumed as 13 GHz, the output QW laser is operating in MLM as presented in Fig. 2(a), and there are three longitudinal modes in individual lasing wavelength. Reducing the reflection bandwidth of narrowband FBG to 6 GHz transformed the laser operation to SLM, and the simulated spectrum of output laser is shown in Fig. 2(b), where there are four lasing wavelengths and only one mode existing in each wavelength. Note that, the linewidth of the simulated spectrum is not authentic here, because the spectral broadening has not been considered in the simulation.

Figure 3 shows the simulated temporal evolution when four wavelengths are lasing simultaneously during the first 200 round trips after the QW laser has reached stable state. The temporal evolution of the QW laser lasing in MLM operation is illustrated in Fig. 3(a) and, as indicated, the output power reaches 10 mW with the average power of 4.5 mW. Nevertheless, the output laser fluctuates below 6 mW with the average power of 3 mW when the QW laser is lasing in SLM operation, as

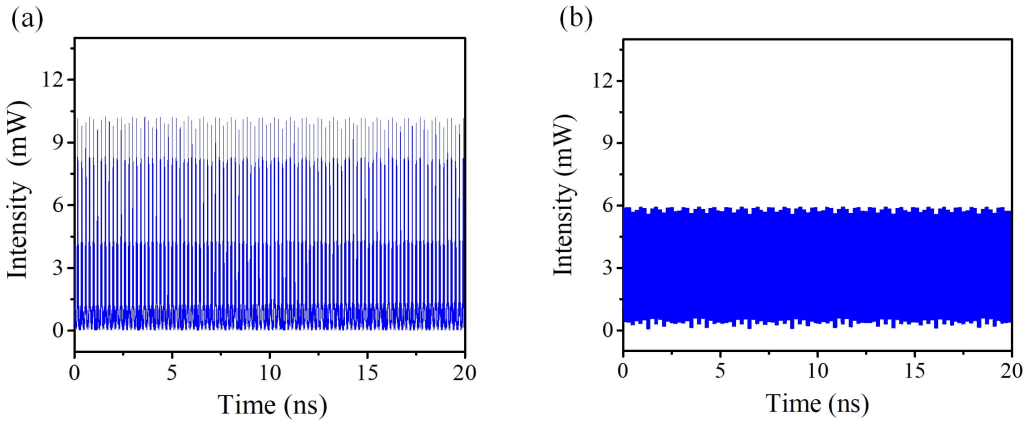

Fig. 3. Simulated temporal evolution in 20 ns of the QW-SFFL in (a) MLM and (b) SLM operation.

displayed in Fig. 3(b). The comparison of the calculated temporal evolutions between the QW-SFFL with MLM and SLM operation clearly indicates that the SLM operation can promote the stability in multi-wavelength fiber laser.

It is also demonstrated from Fig. 3 that a stable solution of the present system can be hardly achieved due to the interactions between four channels. Although the QW laser operates in a steady state, the intensity fluctuation about the average intensity is still exhibited. A useful statistic which described the magnitude of the power fluctuation is the normalized intensity variance (NIV) [26]. After obtaining the temporal evolution of output power in SLM operation, the NIV of QW laser was calculated as 0.42. In order to find out the correlation between the number of lasing wavelengths and the power fluctuation, the NIVs of single- and dual-wavelength laser were calculated. The NIVs of the lasers in single-wavelength operation are 2.98×10^{-9}, 2.14×10^{-10}, 3.03×10^{-9} and 2.51×10^{-10}, respectively, which indicates the single-wavelength lasers are highly stable. The dual-wavelength laser, comprising the first and second wavelengths generated by PM-FBG1 and wideband FBG, has the NIV of 4.90×10^{-7}, analogously, the NIV of the dual-wavelength laser comprising the third and fourth wavelengths is 3.40×10^{-7}. It shows unambiguously that the NIV of a single-wavelength laser is much lower than that of dual- and quad-wavelength laser. Furthermore, as the number of lasing wavelengths is increasing, the disturbance of the output power become larger. Because the interactions among four frequency components generate cross-phase modulation and four-wave mixing, which causes the multiple coupled NLSEs having periodic solutions [24]. If such energy flux is considered from the mathematical viewpoint, oscillation of the obtained solution can be interpreted as a quasi-periodic trajectory in a dynamical system. Fiber resonator cavity is always an ideal platform for exploring and verifying diverse nonlinear dynamics. Hitherto, significant works have been carried out based on the modulation instability with four-wave mixing and cross-phase modulation [25], [27]. However, aside from the effect of cross-phase modulation and four-wave mixing, the mode competition, refer to (1)–(8), also contributes to the quasi-periodic motion of the solution. Revealed by X. Liu *et al.* [28], lasing stability might be improved by further enhancing the nonlinear effect.

According to the modeling and simulation, we confirm that the quad-wavelength laser can be generated in a short linear resonant cavity with a DC-PM-FBG. In order to realize the stable operation of QW laser, single frequency at individual wavelength should be guaranteed in the following experiment.

3. Experimental Setup and Results

Based on the above theoretical model, a QW-SFFL with ultrashort linear cavity was proposed, and the experimental configuration is showed in Fig. 4. Construction of the laser resonant cavity is completed by fusion splicing a wideband FBG having a reflectivity of over 99.5% and a narrowband

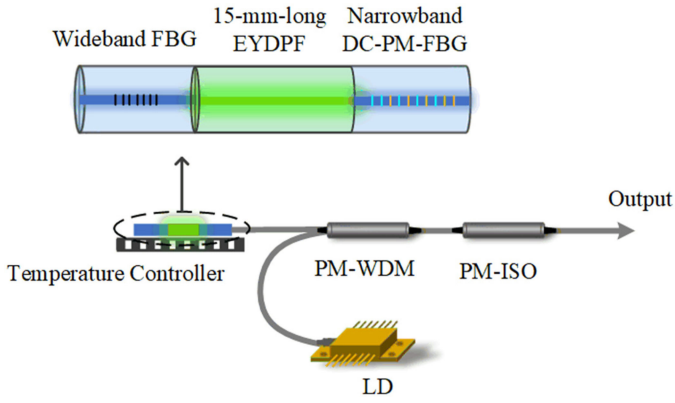

Fig. 4. Experimental setup of the polarization-maintaining quad-wavelength single-frequency fiber laser. EYDPF, Er^{3+}/Yb^{3+} co-doped phosphate fiber; DC-PM-FBG, dual-channel polarization maintaining fiber Bragg grating; LD, laser diode; PM-WDM, polarization maintaining wavelength division multiplexer; PM-ISO, polarization maintaining isolator.

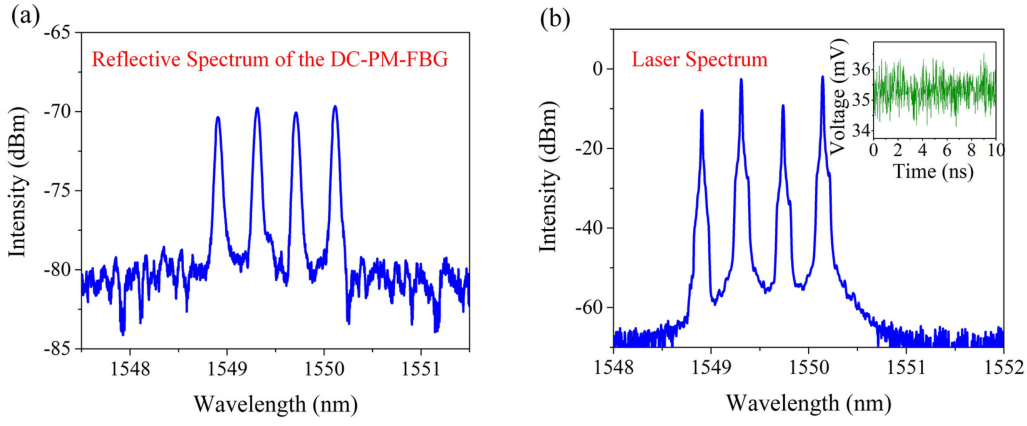

Fig. 5. (a) Reflectivity of the narrowband DC-PM-FBG measured by an amplified spontaneous emission light source. (b) Optical spectrum of the QW-SFFL with a span of 4 nm recorded by an optical spectrum analyzer. Inset is the temporal evolution of QW-SFFL in 10 ns which is obtained by the oscilloscope with a resolution of 20 GHz.

DC-PM-FBG on each end of a 15-mm-long self-developed EYDPF. The commercial DC-PM-FBG is fabricated by engraving two PM-FBGs (PM-FBG1 and PM-FBG2) at the adjacent location on the fiber, and each PM-FBG split into two reflection peaks with two central wavelengths that separated 0.4 nm corresponding to the slow and fast axes of the PM fiber, respectively. The reflection band spacing of two slow axes is 0.8 nm and all the 3-dB bandwidths are less than 0.073 nm. Two reflectivities corresponding to slow axes and fast axes of 65% and 62%, respectively.

This resonant cavity was thermal controlled by a cooling system with a resolution of 0.05 °C. With proper temperature control at around 26 °C, a robust QW laser could be obtained without mode hopping. The QW laser was counter-pumped by a 976-nm single-mode laser diode (LD) through a PM wavelength division multiplexer (PM-WDM). The laser signal output from the PM-WDM and then passed through a both-axis working PM isolator (PM-ISO) that could prevent back reflections.

Figure 5(a) presents the reflectivity of DC-PM-FBG measured by an amplified spontaneous emission light source in 1.5-μm region and there are four reflection bands in one DC-PM-FBG. The output spectrum of the QW laser showed in Fig. 5(b) was recorded by an optical spectrum analyzer with a resolution of 0.02 nm under a pump power of 200 mW, indicating the central wavelengths for

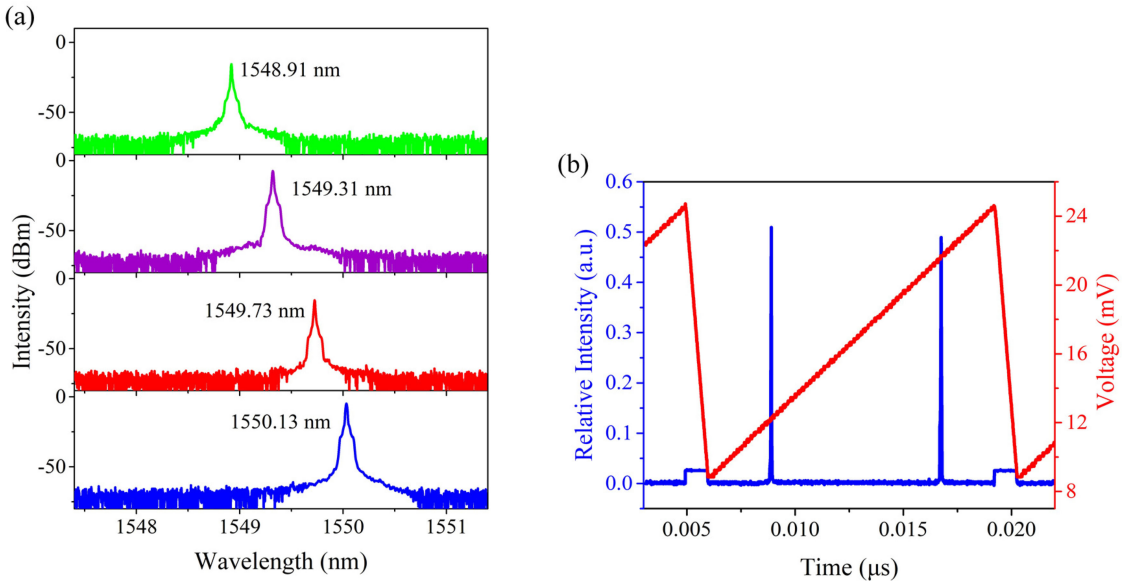

Fig. 6. (a) Separated laser spectra at 1548.91, 1549.31, 1549.73 and 1550.13 nm by using four FBGs with the 3-dB bandwidth of 0.2 nm. (b) Representative of single-frequency performance of QW-SFFL at wavelength of 1550.13 nm.

each peak are 1548.91, 1549.31, 1549.73, and 1550.13 nm, respectively. The first and second laser correspond with the central wavelengths of PM-FBG1, and the third and fourth correspond with the central wavelengths of PM-FBG2. The optical peaks of 1549.31 and 1550.13 nm corresponding to slow axes are 8 dB higher than that of other two lasing wavelengths. This intensity discrepancy is generated because the wavelength-dependent absorption and emission cross section for Er^{3+} are wavelength-dependent in the amplification and propagation processes, which causes the gain to be unequal among each wavelength. Furthermore, the reflectivity of each channel in DC-PM-FBG is different, so the lasers produced by slow axes are dominative in mode competition, consequently, the power disequilibrium is generated among different wavelengths. The experimental output spectrum is consistent with the simulated spectrum.

The inset of Fig. 5(b) illustrates the stability of the QW laser when operating under a pump power of 200 mW that detected by an InGaAs photodetector with the bandwidth of 12.5 GHz and an oscilloscope with the resolution of 20 GHz. The result demonstrates that the slight output power fluctuation is existing in the time domain when four wavelengths are lasing simultaneously. Due to the strong mode competition and modulation instability produced among different wavelengths, the power fluctuation can hardly be eliminated in the nanosecond range.

In an effort to further characterize the performance of individual wavelength, more precise measurements of various aspects of the individual wavelength laser were implemented after being separated by four FBGs with the 3-dB bandwidth of 0.2 nm. The spectra for each lasing wavelength are showed in Fig. 6(a) in which the wavelength spacing is nearly equal and as narrow as 0.4 nm. Then the longitudinal-mode characteristics for each separated wavelength were measured by a scanning Fabry-Perot interferometer having a resolution of 7.5 MHz and a free spectral range of 1.5 GHz. By adjusting the temperature of resonant cavity, the Bragg wavelength of DC-PM-FBG would be shifted and in accord with the center longitudinal mode, then a robust single-frequency operation at each wavelength could be obtained. When the temperature was control at around 26 °C, the SLM operations of individual lasing wavelength were verified, and the representative measurement result for the wavelength of 1550.13 nm is showed in Fig. 6(b).

In addition, the linewidths for individual wavelength were measured by the self-heterodyne method, which involved a 48.8-km fiber delayed Mach-Zehnder interferometer and a 40-MHz fiber-coupled acousto-optical modulator. The linewidth measurements give substantially the similar

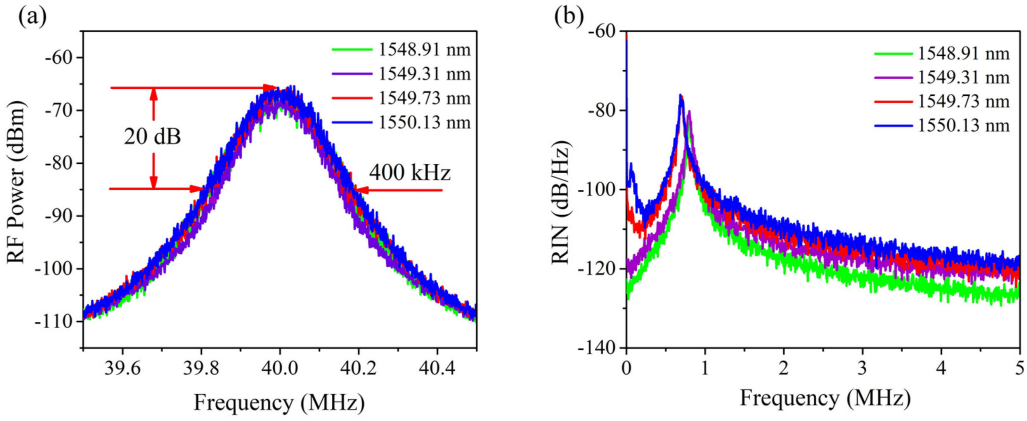

Fig. 7. (a) Linewidth measurements of the QW-SFFL at individual wavelength measured by the self-heterodyne method. (b) RIN of the QW-SFFL at individual wavelength from 0 to 5 MHz.

results for each wavelength, as showed in Fig. 7(a). The 20-dB spectrum widths are measured to be 400 kHz which suggests that the Lorentz linewidths are 20 kHz.

Figure 7(b) elucidates the relative intensity noise (RIN) measured by an InGaAs photoelectric detector with the bandwidth of 150 MHz and the electrical spectrum analyzer. It reveals that the relaxation oscillation peaks of dual wavelengths corresponding to PM-FBG2 are −76 dB/Hz at the frequency of 0.7 MHz, and that of the other two wavelengths are −80 dB/Hz at the frequency of 0.81 MHz. Apart from the relaxation oscillation peaks, the RINs are lower than −113 dB/Hz when frequencies are over 3 MHz. The different frequencies of relaxation oscillation peaks are caused by different cavity lengths between two dual-wavelength lasers because of the limitations of commercial FBG processing technology. In effect, PM-FBG2 deviates from PM-FBG1 by approximately 7 mm. And the relaxation oscillation frequency is pulled to the lower frequency with longer cavity length because the relaxation oscillation frequency is inversely proportional to the photon lifetime, which is increased by transmitting in a longer cavity [29].

4. Conclusions

A compact PM-QW-SFFL by utilizing a 15-mm-long EYDPF in a short-linear cavity has been demonstrated. By modeling the evolution of optical fields with rate equations and NLSEs, the formation and interaction mechanisms of multi-wavelength in SFFL are systematically analyzed. The simulated results indicate that the SLM operation and all-PM structure of QW fiber laser can reduce the instability brought by nonlinear effects. The robust PM-QW-SFFL with the equal wavelength spacing and 20-kHz linewidth at the individual wavelength is achieved. The compact PM-QW-SFFLs are desirable light sources in lidar applications and fiber sensors.

References

[1] C. Weitkamp Ed., *LIDAR: Range-Resolved Optical Remote Sensing of the Atmosphere*. New York, NY, USA: Springer, 2005.
[2] X. Fu *et al.*, "Intensity demodulation based fiber sensor for dynamic measurement of acoustic wave and lateral pressure simultaneously," *IEEE Photon. J.*, vol. 8, no. 6, Dec. 2016, Art. no. 6805713.
[3] C. J. Karlson, F. A. A. Olsson, D. Letalick, and M. Harris, "All-fiber multifunction CW coherent laser radar at 1.55 μm for range speed vibration and wind measurements," *Appl. Opt.*, vol. 39, no. 21, pp. 3716–3726, Jul. 2000.
[4] K. Venkataraayan, S. Askraba, K. Alameh, and C. Smith, "Photonic-based multi-wavelength sensor for object identification," *Opt. Exp.*, vol. 18, no. 4, pp. 3774–3783, Feb. 2010.
[5] U. Sharma, C. Kim, and J. Kang, "Highly stable tunable dual-wavelength Q-switched fiber laser for DIAL applications," *IEEE Photon. Technol. Lett.*, vol. 16, no. 5, pp. 1277–1279, May 2004.

[6] K. Nakagawa, M. de Labachelerie, Y. Awaji, and M. Kourogi, "Accurate optical frequency atlas of the 1.5-μm bands of acetylene," *J. Opt. Soc. Amer. B*, vol. 13, no. 12, pp. 2708–2714, 1996.
[7] N. J. Vasa and M. Singaperumal, "Gas sensors based on superluminescent diodes for combustion monitoring," *Appl. Opt.*, vol. 48, no. 31, pp. G1–G5, 2009.
[8] C. Yang *et al.*, "10.9 W kHz-linewidth one-stage all-fiber linearly-polarized MOPA laser at 1560 nm," *Opt. Exp.*, vol. 21, no. 10, pp. 12546–12551, May 2013.
[9] S. R. Rodrigo, R. A. Herrera, I. Ibañez, A. M. Pinto, M. F. Vallejo, and M. L. Amo, "Multiwavelength fiber ring laser based on optical add-drop multiplexers and a photonic crystal fiber Sagnac interferometer," *Opt. Laser Technol.*, vol. 48, pp. 72–74, Nov. 2013.
[10] H. Ahmad, M. R. K. Soltanian, C. H. Pua, M. Z. Zulkifli, and S. W. Harun, "Narrow spacing dual-wavelength fiber laser based on polarization dependent loss control," *IEEE Photon. J.*, vol. 5, no. 6, Dec. 2013, Art. no. 1502706.
[11] W. Li, F. Kong, and J. Yao, "Stable and frequency-hopping-free microwave generation based on a mutually injection-locked optoelectronic oscillator and a dual-wavelength single-longitudinal-mode fiber laser," *J. Lightw. Technol.*, vol. 32, no. 21, pp. 3572–3577, Nov. 2014.
[12] Q. Zhao *et al.*, "Broad-bandwidth near-shot-noise-limited intensity noise suppression of a single-frequency fiber laser," *Opt. Lett.*, vol. 41, no. 7, pp. 1333–1335, Apr. 2016.
[13] S. Mo *et al.*, "600-Hz linewidth short-linear-cavity fiber laser," *Opt. Lett.*, vol. 39, no. 20, pp. 5818–5821, Oct. 2014.
[14] E. Desurvire, J. L. Zyskind, and J. R. Simpson, "Spectral gain hole-burning at 1.53 μm in erbium-doped fiber amplifiers," *IEEE Photon. Technol. Lett.*, vol. 2, no. 4, pp. 246–248, Apr. 1990.
[15] X. Liu *et al.*, "Switchable and tunable multiwavelength Erbium-doped fiber laser with fiber Bragg gratings and photonic crystal fiber," *IEEE Photon. Technol. Lett.*, vol. 17, no. 8, pp. 1626–1628, Aug. 2005.
[16] Y. Zhang *et al.*, "Dual-wavelength passively q-switched single-frequency fiber laser," *Opt. Exp.*, vol. 24, no. 14, pp. 16149–16155, Jul. 2016.
[17] Y. G. Han, T. V. A. Tran, and S. B. Lee, "Wavelength-spacing tunable multiwavelength erbium-doped fiber laser based on four-wave mixing of dispersion-shift fiber," *Opt. Lett.*, vol. 31, no. 6, pp. 697–699, Mar. 2006.
[18] T. Zhu *et al.*, "Tunable dual-wavelength fiber laser with ultra-narrow linewidth based on Rayleigh backscattering," *Opt. Exp.*, vol. 24, no. 2, pp. 1324–1330, Jan. 2016.
[19] C. Yang *et al.*, "High-power and near-shot-noise-limited intensity noise all-fiber single-frequency 1.5 μm MOPA laser," *Opt. Exp.*, vol. 25, no. 11, pp. 13324–13331, Jun. 2017.
[20] S. Xu, Z. Yang, Z. Feng, Q. Zhang, Z. Jiang, and W. Xu, "Efficient fiber amplifiers based on a highly Er^{3+}/Yb^{3+} codoped phosphate glass-fiber," *Chin. Phys. Lett.*, vol. 26, no. 4, Sep. 2009, Art. no. 47806.
[21] T. Liu, Z. M. Yang, and S. Xu, "3-Dimensional heat analysis in short-length Er^{3+}/Yb^{3+} co-doped phosphate fiber laser with upconversion," *Opt. Exp.*, vol. 17, no. 1, pp. 235–247, Jan. 2009.
[22] S. Turitsyn *et al.*, "Modeling of CW Yb-doped fiber lasers with highly nonlinear cavity dynamics," *Opt. Exp.*, vol. 19, no. 9, pp. 8394–8405, Apr. 2011.
[23] W. Liu, W. Kuang, L. Huang, and P. Zhou, "Modeling of the spectral properties of CW Yb-doped fiber amplifier and experimental validation," *Laser Phys. Lett.*, vol. 12, Mar. 2015, Art. no. 045104.
[24] G. P. Agrawal, *Nonlinear Fiber Optics*. New York, NY, USA: Academic, 2012.
[25] K. W. Chow, K. K. Y. Wong, and K. Lam, "Modulation instabilities in a system of four coupled, nonlinear Schrödinger equations," *Phys. Lett. A*, vol. 372, no. 25, pp. 4596–4600, May 2008.
[26] R. Frehlich, "Simulation of laser propagation in a turbulent atmosphere," *Appl. Opt.*, vol. 39, no. 3, pp. 393–397, Jan. 2000.
[27] D. F. Grosz, C. Mazzali, S. Celaschi, A. Paradisi, and H. L. Fragnito, "Modulation instability induced resonant four-wave mixing in WDM systems," *IEEE Photon. Technol. Lett.*, vol. 11, no. 3, pp. 379–381, Mar. 1999.
[28] X. Liu, X. Zhou, and C. Lu, "Four-wave mixing assisted stability enhancement: Theory, experiment, and application," *Opt. Lett.*, vol. 30, no. 17, pp. 2257–2259, Sep. 2005.
[29] Y. Shevy, D. Shevy, R. Lee, and D. Provenzano, "Slow light laser oscillator," in *Proc. Opt. Fiber Commun. Conf.*, 2010, Paper OThQ6.